

# A Hybrid Deep Feature-Based Deformable Image Registration Method for Pathological Images

Chulong Zhang<sup>1,3</sup>, Yuming Jiang<sup>2</sup>, Na Li<sup>4</sup>, Zhicheng Zhang<sup>5</sup>, Md Tauhidul Islam<sup>2</sup>, Jingjing Dai<sup>1</sup>, Lin Liu<sup>1</sup>, Wenfeng He<sup>1</sup>, Wenjian Qin<sup>1</sup>, Jing Xiong<sup>1</sup>, Yaoqin Xie<sup>1</sup> and Xiaokun Liang<sup>1\*</sup>

<sup>1\*</sup>Shenzhen Institute of Advanced Technology, Chinese Academy of Sciences, Shenzhen, 518055, Guangdong, China.

<sup>2</sup>Department of Radiation Oncology, Stanford University, Stanford, 94305, CA, USA.

<sup>3</sup>School of Mathematics, Sun Yat-sen University, Guangzhou, 510275, Guangdong, China.

<sup>4</sup>Department of Biomedical Engineering, Guangdong Medical University, Dongguan, 523808, Guangdong, China.

<sup>5</sup>Xiaohu Healthcare ByteDance, Guangzhou, 510000, Guangdong, China.

\*Corresponding author(s). E-mail(s): [xk.liang@qq.com](mailto:xk.liang@qq.com) / [xk.liang@siat.ac.cn](mailto:xk.liang@siat.ac.cn);

## Abstract

Pathologists need to combine information from differently stained pathological slices to obtain accurate diagnostic results. Deformable image registration is a necessary technique for fusing multi-modal pathological slices. This paper proposes a hybrid deep feature-based deformable image registration framework for stained pathological samples. We first extract dense feature points and perform points matching by two deep learning feature networks. Then, to further reduce false matches, an outlier detection method combining the isolation forest statistical model and the local affine correction model is proposed. Finally, the interpolation method generates the DVF for pathology image registration based on the above

matching points. We evaluate our method on the dataset of the Non-rigid Histology Image Registration (ANHIR) challenge, which is co-organized with the IEEE ISBI 2019 conference. Our technique outperforms the traditional approaches by 17% with the Average-Average registration target error (rTRE) reaching 0.0034. The proposed method achieved state-of-the-art performance and ranking it 1 in evaluating the test dataset. The proposed hybrid deep feature-based registration method can potentially become a reliable method for pathology image registration.

**Keywords:** Deformable Image Registration, Deep Learning, Deep Feature-Based Registration, Pathological Images

## 1 Introduction

Registration of pathological images is vital for current histology image analysis and decision-making. In clinics, the registration of pathology images is commonly performed based on the 3D reconstruction of scanned 2D thin slices, creating a high-resolution pathological image. The fusing technique is then performed on separately stained slices [1]. The challenge of this process is that pathology images are characterized by high resolution, large deformation, repetition, and complex textures [2]. Examples of some pathological images of different sites are shown in Figure 1.

The conventional methods used for medical image registration are not suitable for pathological images [3–7] due to the properties discussed earlier. Traditional medical image registration techniques include intensity-based, feature-based, and segmentation-based methods. In recent years, researchers have developed a number of non-rigid registration methods, such as bUnwarpJ [3], NiftyReg [4], RVSS [3], ANTs [5], DROP [6], and Elastix [7]. The above methods were tested in the Automated Non-Rigid Histological Image Registration (ANHIR) challenge dataset [2, 8, 9]. However, the results obtained were unsatisfactory.

Fraunhofer MEVIS was the method with the best performance on the ANHIR dataset [2, 10]. The authors provide a non-rigid registration framework using normalized gradient fields (NGF) as a similarity measure. This framework includes the steps of initial rotation search, iterative affine, and b-spline-based registration. A deep learning technique was also proposed for analyzing the ANHIR dataset [2, 11]. The researchers optimized the network using manually defined signposts after re-sampling the images to a relatively low resolution. Although the technique is faster than other competing methods, the accuracy of this method is not convincing. Subsequently, an unsupervised medical image registration network based on deep learning was proposed [1, 12–15]. The framework is separated into three sections: initial alignment, affine alignment, and non-rigid registration. They employ global NCC for

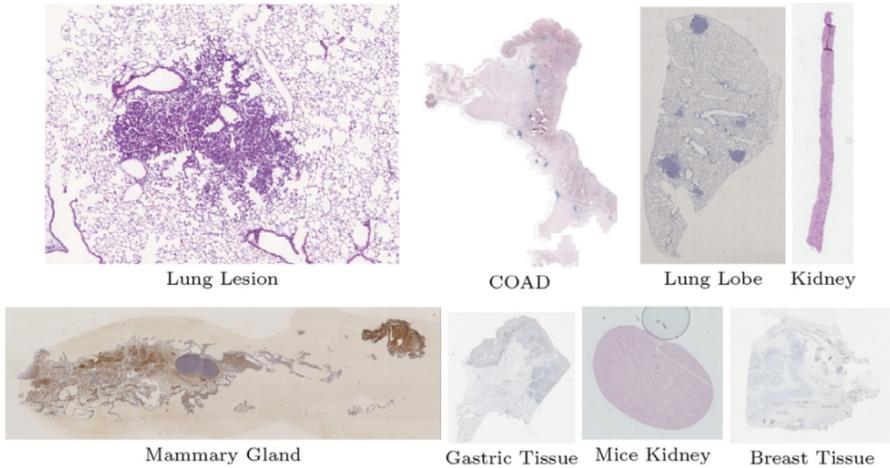


**Fig. 1** Examples of pathological images of each site.

initial alignment and affine registration and patch-based normalized cross-correlation (NCC) for non-rigid registration. The smooth of the deformation vector field is used as the regularization term for the non-rigid registration. Although the approach significantly improved registration speed, it failed to deliver high accuracy.

In intensity-based registration, iterative search strategies or neural networks are employed to optimize similarity metrics, including mean square error (MSE) and NCC, et al. As a result, the deformation vector fields (DVF) corresponding to the fixed and moving images are obtained. Another alternative is the feature-based registration technique. Its implementation includes the following steps: firstly, feature points of the image are obtained, and feature descriptors are used to describe the feature points; then matching is performed according to the descriptors; finally, transform fields are generated by interpolation after point matching. The main drawback of learning-based registration methods depending on similarity measures is that they still inherit the iterative nature of traditional deformable image registration (DIR) frameworks and share identical or similar objective functions. However, traditional methods can minimize this objective function for each case separately [1]. As a result, to achieve high accuracy in the registration process, we have to develop a framework with multiple loss functions than the traditional iterative-based techniques. A feature point matching approach based on deep learning might be a potential solution.

Feature-based methods work in both manual extraction and deep learning-based registration approaches [16]. Traditional methods such as SIFT [17], ORB [18] use gradient, grayscale, and other information to manually design feature points for matching. Nevertheless, this technique concentrates on local

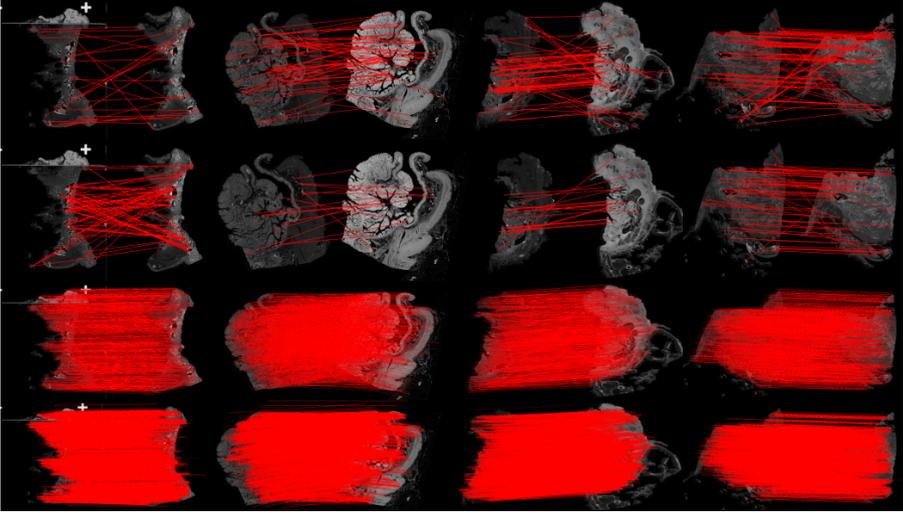


**Fig. 2** Comparison of deep learning feature-based methods and manual feature-based image matching methods. From top to bottom are SIFT, ORB, SuperPoint + SuperGlue, and COTR, where SIFT and ORB are classical manual feature-based methods, while SuperPoint + SuperGlue and COTR are deep learning feature-based methods.

features and yields sparse feature points. In contrast, deep learning-based feature extraction algorithms consider characteristics of diverse sizes and scales, contributing to more comprehensive features. There are two types of deep learning techniques: detector-based and detector-free approaches [19]. Whether a feature extraction network is required determines how these two categories vary from one another. The detector-based approach uses the response values of the network to detect interest points. It constructs descriptors using features extracted by a convolutional neural network (CNN) and U-Net, such as SuperPoint [20], DISK [21]. These interest points and descriptors then match and get the corresponding feature pairs. Detector-free techniques, such as Correspondence Transformer-based image matching network (COTR) [22] and LOFTR [19], employ the designed network for end-to-end matching without requiring a dedicated detector to identify interest sites.

Figure 2 depicts the difference between manual feature approaches and deep learning methods. The upper two rows include SIFT and ORB, the most widely utilized feature points for manual learning. The bottom two rows present the outputs of SuperPoint + SuperGlue [23] (detector-based) and COTR (detector-free).

However, pre-matching or affine transformation of medical images based on traditional hand-crafted feature points (SIFT, SURF [24], ORB) is common. Recently, some work has proven that feature-based approaches, particularly those based on deep learning, perform well for cross-modality medical image matching [25]. The study states the results of several feature matching methods for typical multi-modal images in medical research fields such as MRI-PET,

CT-SPECT, etc. Additionally, it demonstrates that implementing deep feature approaches for medical image registration is viable and beneficial.

Two main issues limit the accuracy of conventional feature-based approaches for registration: 1) feature points and matched point pairs are excessively sparse, resulting in unacceptable errors between the interpolated estimated DVF and the real DVF. 2) there might be substantial mismatches, which severely diminish the accuracy of the DVF. We propose a hybrid deep learning feature-based registration framework to tackle these challenges. We integrate detector-based and detector-free networks to extract features and sufficiently match dense pairs of feature points. In addition, we construct an outlier detection module for mistake matching pairs detection based on local and global consistency of medical images.

We validate our approach on the ANHIR dataset. We observed that employing model parameters pre-trained for natural image datasets during inference achieved fairly good performance. Furthermore, we combine the robust results of two separate networks, the outputs after anomaly detection as pseudo-labels, and the landmarks supplied in the dataset as ground truth to co-construct the training set to fine-tune the network. These further enhance the network performance. We have three major contributions.

- To solve the problem of sparse and erroneous matching points in traditional feature-based medical image registration, we proposed a hybrid deep feature-based image registration method for pathological image registration. The proposed method achieved state-of-the-art performance.
- In our experiments, we found that the feature matching network trained based on natural images can be well migrated to the scenes of medical images and obtained quite a high accuracy. The results inspired us to use the large dataset in natural images to solve the tricky problems in medical images.
- We converted the erroneous matching problem into a global and local outlier detection problem. An outlier detection method combining the isolation forest statistical model and the local affine correction model was proposed.

## 2 Method

We provide a framework for hybrid deep feature-based registration. Our framework is separated into feature point pair generation, anomaly matching detection, and DVF generation. In our initial inference procedure, we employ pre-trained models that have been learned directly on the natural image dataset. The outputs of the model and the landmarks in the training set are combined with fine-tuning the model, yielding the newly trained model. The new model provides more accurate results. Figure 3 depicts the detailed flow chart. We extract various feature point pairs in the feature point pairs generation module. Feature point pair A:  $(x_m, y_m, x_m^1, y_m^1), m \in \mathcal{M}$  and feature point pair B:  $(x_n, y_n, x_n^2, y_n^2), n \in \mathcal{N}$ ,  $(x_m, y_m)$  are the coordinates of the feature points in the source image,  $(x_m^1, y_m^1)$  and  $(x_n^2, y_n^2)$  are the coordinates of the feature point pairs in the predicted target image.

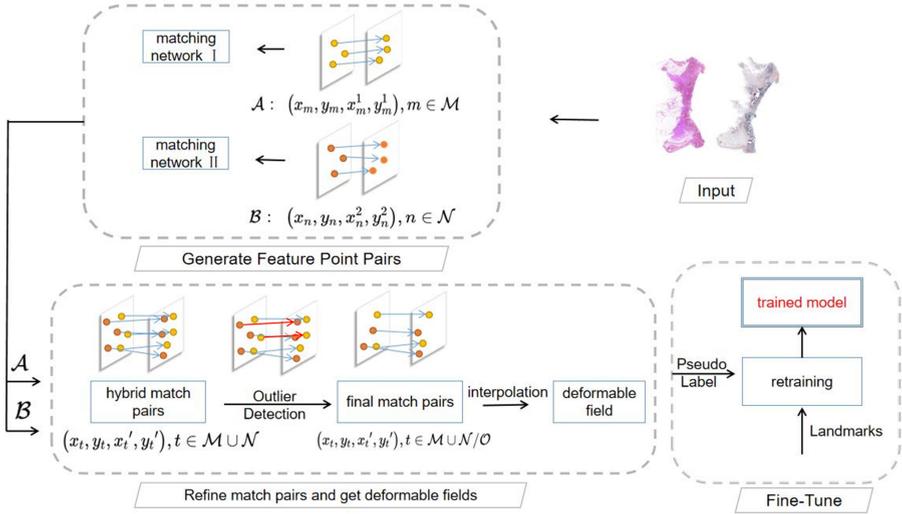


**Fig. 3** Workflow of the proposed method. **Generate Feature Point Pairs:** We extract multiple pairs of feature points from different networks. **Refine match pairs and get deformable fields:** The point pairs are combined and passed into the outlier detection module. Finally, new point pairs are obtained, and the DVF is generated by interpolation. **Fine-Tune:** First, we employ a pre-trained model in natural images on our inference. Then, we use the inference output to construct pseudo-labels and landmarks to train the network together. The final trained model is obtained to achieve more accurate results.

We integrate the feature point pairs produced by the two networks to create new point pairs  $(x_t, y_t, x_t', y_t'), t \in \mathcal{M} \cup \mathcal{N}$ . An outlier diagnosis module is proposed in the anomaly matching detection. The DVF generation module combines an isolated forest model and a local affine correction model. The local affine correction model is based on global and local image consistency principles. The anomalous matches are eliminated while using this strategy. We employ the final obtained point pairs as pseudo-labels to fine-tune the original model together with the ground-truth point pairs provided by the dataset. As a result, the final obtained model performs more accurate inference.

## 2.1 matching network I

Matching network I is a COTR. First, the two input images are resized to  $256 \times 256$ . Subsequently, the two are combined side-by-side using the same CNN backbone extracted to dimension  $16 \times 16 \times 256$  feature map  $\mathcal{E}$ . Subsequently, the coordinate function is  $\Omega$  encoded via the position encoder  $\mathcal{P}$ , and the above two are combined to obtain the contextual feature map  $c \in \mathcal{R}_{16 \times 32 \times 256}$ . The network architecture of COTR is shown in Figure 4.

Then  $c$  is fed to the transformer encoder  $\mathcal{T}_{\mathcal{E}}$ , and the position-encoded  $\mathbf{x}$  is decoded by the transformer decoder  $\mathcal{T}_{\mathcal{D}}$ . Finally, the network output  $\mathbf{x}'$  is obtained after an MLP, and the above process can be described in the following form.

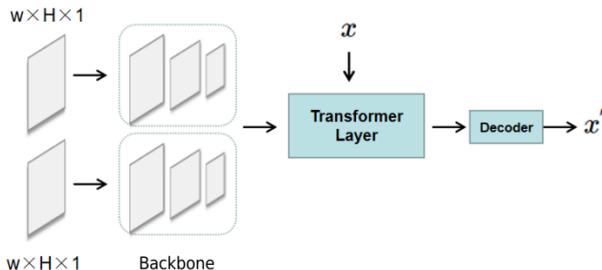


**Fig. 4** Matching network I comprises the feature extraction and Transformer module. After approaching the CNN network to extract features, the two images go through an encoding-decoding-decoding procedure to get the coordinates  $x$  in the fixed image corresponding to  $x'$  in the moving image.

$$x' = \mathcal{F}_{\Phi}(x | I, I') = \mathcal{D}(\mathcal{T}_{\mathcal{D}}(\mathcal{P}(x), \mathcal{T}_{\mathcal{E}}(c))) \quad (1)$$

This network can obtain highly accurate matching relationships by iterating using  $\mathcal{F}_{\Phi}$ . The initial value of the next iteration is a scaled-up version of the previous prediction after cropping, scaling the image down to  $256 \times 256$ . This way, we can achieve matching at any scale and fully use the information at each scale.

The goal of the network is to minimize the error in the matching as well as the mutual consistency error of the matches. The training set for this network and Matching Network II consists of pairs of natural image and the corresponding relationships derived by calculating camera parameters. No specific training is required for the pathological images.

$$\arg \min_{\Phi} \mathbb{E}_{(x, x', I, I') \sim \mathcal{D}} \mathcal{L}_{\text{corr}} + \mathcal{L}_{\text{cycle}} \quad (2)$$

$$\mathcal{L}_{\text{corr}} = \|x' - \mathcal{F}_{\Phi}(x | I, I')\|_2^2 \quad (3)$$

$$\mathcal{L}_{\text{cycle}} = \|x - \mathcal{F}_{\Phi}(\mathcal{F}_{\Phi}(x | I, I') | I, I')\|_2^2 \quad (4)$$

Where  $\mathcal{D}$  denotes the training set with true matching relationships;  $\mathcal{L}_{\text{corr}}$  denotes the error in matching estimates, and  $\mathcal{L}_{\downarrow\uparrow\downarrow\uparrow}$  denotes the mutual consistency error.

The network needs to be pre-trained on the natural image dataset MegaDepth [26]. The dataset contains 200 models of landmarks worldwide with dense 3D reconstruction, while 150,000 reconstructed images are presented. After filtering, 130,000 usable images are retained; out of these 130,000 images, about 100,000 are absolute depth data, and 30,000 are relative depth data. We can get the one-to-one correspondence of the position relationship of the image pairs in the dataset for training.

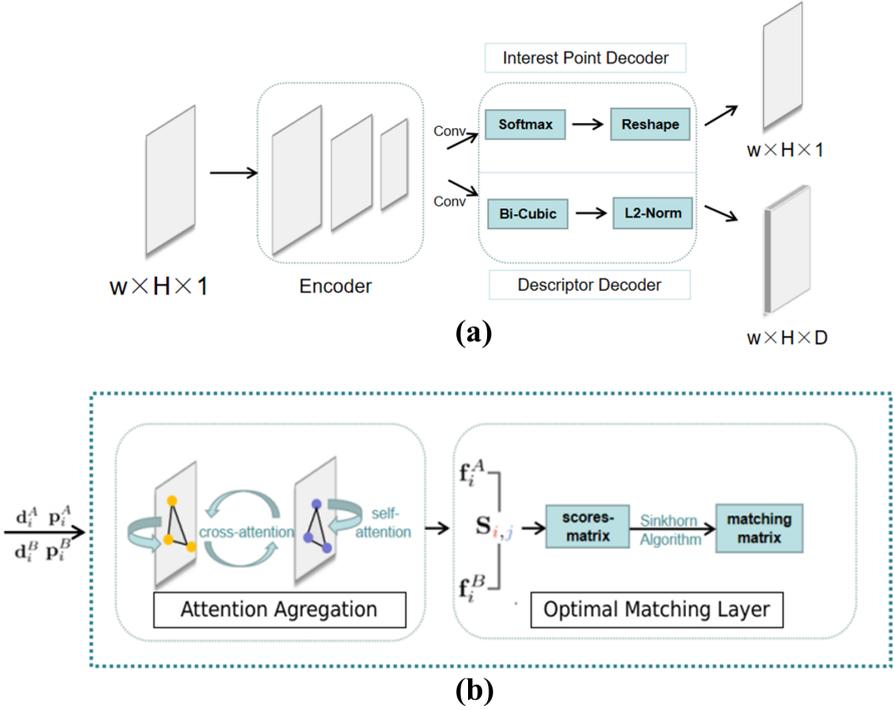


**Fig. 5** Two parts of matching network II. The first part is SuperPoint (a), a self-supervised feature point extraction and descriptor construction network. The second part is SuperGlue (b), a feature matching network based on graph networks.

## 2.2 matching network II

The matching network comprises two networks: a feature point extraction network and a feature point matching network. The former is a self-supervised network (SuperPoint) for extracting feature points and calculating descriptors, while the latter is a graph network-based image matching network (SuperGlue).

SuperPoint is a deep feature point extraction and descriptor generation network. The structure is shown in Figure 5. Feature point detection network is a decoder. It determines the probability of each pixel in an image being a feature point by estimating its likelihood. A decoder is also a component of the descriptor detection network. First, a semi-dense descriptor is learned, then a bi-trivial interpolation is used to acquire the entire descriptor. Finally, L2-normalizes are performed to generate a unit-length descriptor. The entire loss function is presented as follows:

$$\mathcal{L}(X, X'; Y'; D, D'; S) = \mathcal{L}_p(X, Y) + \mathcal{L}_d(X', Y') + \lambda \mathcal{L}_d(D, D', S) \quad (5)$$

Where  $\mathcal{L}_p$  is the loss function for the feature points, and  $\mathcal{L}_d$  is the loss function for the descriptors, with coefficients to balance the two weights.

SuperGlue is a feature matching network based on Graph Neural Networks and attention mechanisms. Our high-dimensional perceptron performs location encoding by encoding the location information  $\mathbf{p}_i = (x, y, c)$  into the descriptor  $\mathbf{d}$ . Then, feeding the encoded descriptor into a graph network based on self-attention and cross-attention mechanisms after two attention layers: (i) self-attention, which enhances the receptivity of local descriptors; and (ii) cross-attention, which enables cross-image information flow. Finally, the Sinkhorn Algorithm is used to obtain the optimal matching matrix.

The SuperPoint network is trained with generated pseudo-ground truth data and image pairs obtained by deforming many images on the MS-COCO [27] dataset. SuperGlue uses many indoor paired images provided by the ScanNet [28] dataset as the training set. Both networks I and II are trained with many paired images collected or generated by the camera as the ground truth, enabling the network to learn how to identify the one-to-one mapping relationship between two images.

## 2.3 Outlier Detection Model

An outlier detection is proposed to tackle the problem of detecting the wrong point pair. For example, we commonly employ RANSAC [29, 30] to eliminate outliers in image matching. On the other hand, RANSAC is based on the simple premise that all points in an image meet the same Homography or affine transformation, which is incorrect in the case of sophisticated histology image deformations.

We then assume the following hypotheses for point displacements in pathological images: 1) The overall displacement of points in the whole image is consistent, i.e., the direction and distance of the displacements of all points in the image will not differ too much, which may be demonstrated by the fact that a simple affine transform estimate is adequate to reach high accuracy. 2) The local distortion of the image will not vary too much, i.e., the displacement of a point and the displacement near that point should be consistent. The overall consistency and local consistency are visibly illustrated in Figure 6. Based on the above, we build an Isolation Forest statistical model [31, 32] and a Local affine correction model for outlier detection. We use the Isolation Forest model to solve the global consistency problem. We employ  $s_i = (\Delta x, \Delta y)$  to signify the displacement of the predicted coordinates from the initial coordinates.

$$\Delta x = x'_t - x_t, \Delta y = y'_t - y_t \quad (6)$$

Then we obtain the set of displacements of the whole image feature points as

$$S = \{s_1, \dots, s_n\} \quad (7)$$

According to our hypothesis, the erroneously matched points represent set S's outliers. We randomly choose the hyperplane and recursively split the data set S until any of the following requirements are fulfilled. (1) the tree achieves the maximum height; (2) there is only one sample on the node; (3) all features

of the samples on the node are the same. The relationship between the height limit  $l$  of the tree and the number of sub-samples  $\psi$  is  $l = \text{ceiling}(\log_2(\psi))$ .

The iForest model consists of two steps: the training phase, which forms isolated trees from sub-samples of the training set, and the testing phase, which computes anomaly scores for each test sample using isolated trees.

In the training phase, the iTree is built by recursively separating the training set until all samples are isolated or the tree has reached the given height. The pseudo-code is as follows.

---

Algorithm 1 :  $iF_{\text{orest}}(S, t, \psi)$

---

Inputs:  $S$  - input data,  $t$  - number of trees,  $\psi$  - sub-sampling size

Output: a set of  $t$  Trees

- 1: Initialize Forest
  - 2: set height limit  $l = \text{ceiling}(\log_2 \psi)$
  - 3: for  $i = 1$  to  $t$  do
  - 4:    $S' \leftarrow \text{sample}(S, \psi)$
  - 5:    $F_{\text{orest}} \leftarrow F_{\text{orest}} \cup i\text{Tree}(S', 0, l)$
  - 6: end for
  - 7: return Forest
- 

---

Algorithm 2 :  $i\text{Tree}(S, e, l)$

---

Inputs:  $S$  - input data,  $e$  - current tree height,  $l$  - height limit

Output: an iTree

- 1: if  $e \geq l$  or  $S \leq 1$  then
  - 2:   return  $\text{exNode}\{\text{Size} \leftarrow S\}$
  - 3: else
  - 4:   let  $Q$  be a list of attributes in  $S$
  - 5:   randomly select an attribute  $q \in Q$
  - 6:   randomly select a split point  $p$  from  $\max$  and  $\min$  values of attribute  $q$  in  $S$
  - 7:    $S_l \leftarrow \text{filter}(S, q < p)$
  - 8:    $S_r \leftarrow \text{filter}(S, q \geq p)$
  - 9:   return  $\text{inNode}\{\text{Left} \leftarrow i\text{Tree}(S_l, e + 1, l),$
  - 10:    $\text{Right} \leftarrow i\text{Tree}(S_r, e + 1, l),$
  - 11:    $\text{SplitAtt} \leftarrow q,$
  - 12:    $\text{SplitValue} \leftarrow p\}$
  - 13: end if
- 

Then the empirical value of the number of sub-samples  $\psi$  tree with the number limit  $t$  can be obtained. From there, isolated samples are obtained by calculating the anomaly score of the test sample by the expected path length  $E(h(x))$ .  $h(x)$  is the number of edges passed from the root node to the leaf nodes of the iTree. Finally, we utilize the average path length  $c(n)$  of the tree

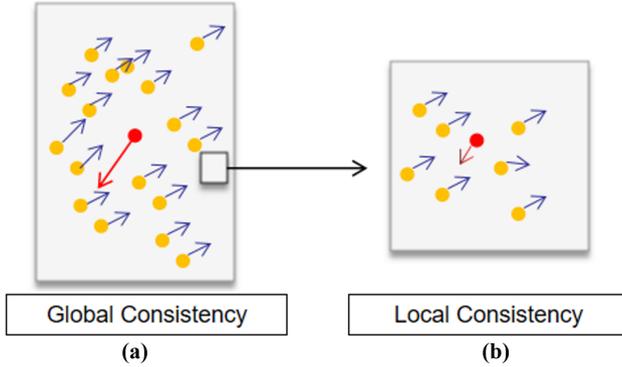


**Fig. 6** The following two cases are considered as the displacement of feature points is anomalous, 1) the displacement of feature points is too different from the global displacement, and 2) the displacement of feature points is too different from the displacement of other feature points of the local image. (a) represents global consistency and (b) represents local consistency.

and  $E(h(x))$  to generate the anomaly scores of the samples  $s(x, n) = 2^{-\frac{E(h(x))}{c(n)}}$ , from which we extract the anomaly values.

The specific algorithm is as follows.

---

Algorithm 3: PathLength ( $s, T, e$ )

---

Inputs :  $s$  - an instance,  $T$ -an iTree,  $e$  - current path length;  
to be initialized to zero when first called

Output: path length of  $s$

- 1: if  $T$  is an external node then
  - 2: return  $e + c(T.size) \{c(\cdot)$  is defined in Equation 1 }
  - 3: end if
  - 4:  $a \leftarrow T.splitAtt$
  - 5: if  $s_a < T.splitValue$  then
  - 6: return PathLength ( $s, T.left, e + 1$ )
  - 7: else  $\{s_a \geq T.splitValue\}$
  - 8: return PathLength ( $s, T.right, e + 1$ )
  - 9: end if
- 

We filter out those sample points significantly different from the global displacement with the above algorithm. Nonetheless, the local anomaly problem in Hypothesis 2 has not been addressed. Therefore, we propose a local affine correction model to conquer this challenge.

First, we sample the feature points in the image randomly and evenly. Then, the sampled point set is constructed as a triangular dissection to lay out the triangular shape of the pathological image. The schematic diagram is shown in Figure 7. The competence of each triangle to construct an affine transformation depending on the displacement of feature points is readily ascertained.

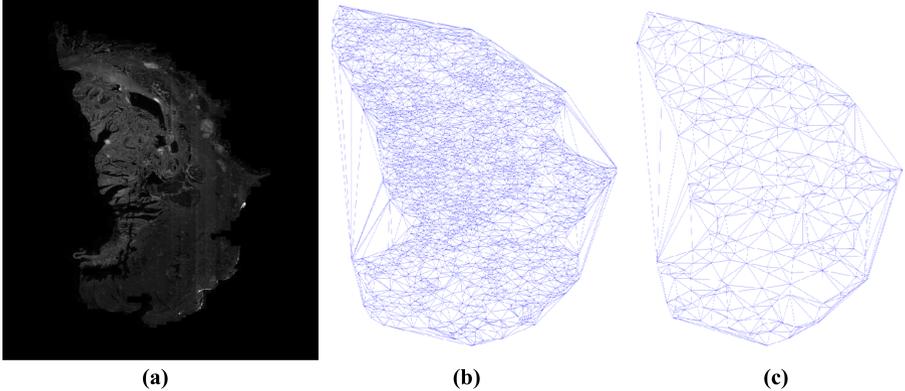


**Fig. 7** Triangle dissection results before and after sampling the feature points on the pathology image, where (b) and (c) represent the triangular dissection results before and after down-sampling of the original image (a). We formed triangles that spread over the pathology image after down-sampling. Each triangle may correspond to an affine transformation, and the points covered in the triangle should match the affine transformation of that triangle.

Therefore, the points covered by the triangles should mainly fulfill the affine transform if these transformations of points are valid.

We allow the point pair formed by some pair and the corresponding point be  $(x_t, y_t, x'_t, y'_t)$ , and the point pair obtained by the affine transformation covering that point at the  $i$ th sampling is  $(x_t, y_t, \hat{x}'_{ti}, \hat{y}'_{ti})$ , then we note that

$$s_t = \sum_{i=0}^n \sqrt{(x'_t - \hat{x}'_{ti})^2 + (y'_t - \hat{y}'_{ti})^2} \quad (8)$$

$s_t$  is the anomaly score of a point after  $n$  times of sampling. We discard the points with high anomaly scores after multiple sampling to obtain the matching points that satisfy local consistency.

## 2.4 Fine-Tune Mouldle

We use the final matches obtained above and the paired landmarks given by the training set to construct a new training set based on the structural features of COTR.

Since the input image of the COTR network is only  $256 \times 256$ , we use the iterative method to perform inference in multi-scale images, as shown in Figure 10. We down-sample the image after getting the previous inference result and crop the image with the inference point as the center to get a new image for iterative inference. This operation enables the algorithm to obtain accurate matching results on large-scale images. We use both the ground truth given in the dataset and the final match obtained in the previous inference process as the dataset. Since the final results obtained in the previous model are more accurate and robust than those obtained by a single COTR network, the pseudo-labels enhance the robustness of the model here. We constructed

**Table 1** Quantitative results evaluated on the ANHIR dataset

	Average-Average rTRE	Average-Median rTRE	Median-Average rTRE	Median-Median rTRE	Max-Average rTRE	Max-Median rTRE
ALL						
Ours	<b>0.0035</b>	<b>0.0022</b>	<b>0.0025</b>	<b>0.0016</b>	0.0258	0.0170
SuperPoint only	0.0056	0.0031	0.0032	0.0021	0.0397	0.0225
COTR only	0.0059	0.0028	0.0035	0.0019	0.0546	0.0245
SFG* [33]	0.0056	0.0024	0.0045	<b>0.0016</b>	0.0240	<b>0.0156</b>
MEVIS[10]	0.0043	0.0028	0.0028	0.0018	0.0251	0.0188
AGH[4]	0.0073	0.0032	0.0036	0.0017	0.0290	0.0214
UPENN[35]	0.0041	0.0029	0.0029	0.0019	<b>0.0238</b>	0.0224
DeepHistReg*[1]	0.0060	0.0033	0.0047	0.0019	0.0239	0.0224
CKVST[2]	0.0042	0.0026	0.0027	0.0023	0.0239	0.0189
TUNI[2]	0.0063	0.0031	0.0048	0.0021	0.0287	0.0204
TEST						
Ours	<b>0.0037</b>	<b>0.0023</b>	<b>0.0026</b>	<b>0.0017</b>	0.0277	<b>0.0183</b>
SFG*	0.0082	0.0026	0.0070	<b>0.0017</b>	0.0286	<b>0.0183</b>
MEVIS	0.0044	0.0027	0.0029	0.0018	0.0251	0.0188
AGH	0.0072	0.0031	0.0057	<b>0.0017</b>	0.0251	0.0188
UPENN	0.0041	0.0029	0.0029	0.0019	<b>0.0239</b>	0.0190
DeepHistReg*	0.0061	0.0030	0.0047	0.0019	0.0276	0.0197
CKVST	0.0042	0.0026	0.0027	0.0023	0.0239	0.0189
TUNI	0.0063	0.0031	0.0048	0.0021	0.0287	0.02045

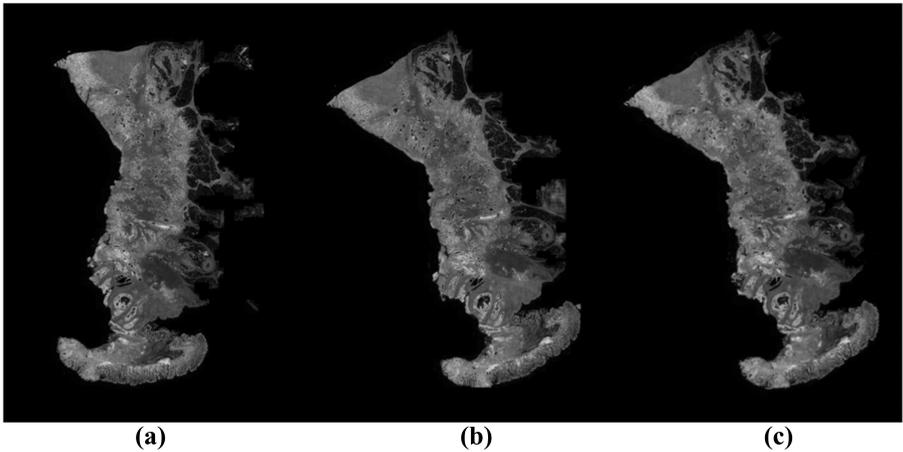


**Fig. 8** An example of the alignment of a pair of images on the ANHIR dataset is provided in Fig, where (a) (b) (c) are the source image, the target image, and the transformed source image, respectively. After the deformation length is applied to the source image, we can observe the comparison with the target image.

different levels of paired images, as shown in Figure 10. Training is performed using pseudo-labels and real labels together.

The new loss function is

$$\arg \min_{\Phi} \mathbb{E}_{(\mathbf{x}, \mathbf{x}', I, I') \sim D} (\mathcal{L}_{\text{corr}} + \mathcal{L}_{\text{cycle}})_{\text{Pseudo-Label}} + (\mathcal{L}_{\text{corr}} + \mathcal{L}_{\text{cycle}})_{\text{Label}} \quad (9)$$

After fine-tuning, the model has been significantly improved.

### 3 Results

The source and target images are fed into the two networks. The final matched point pairs are retrieved after anomaly matching detection. We interpolate the collected matches to obtain the dense DVF. Finally, the DVF is applied to the source image to obtain the transformed image, depicted in Figure 8.

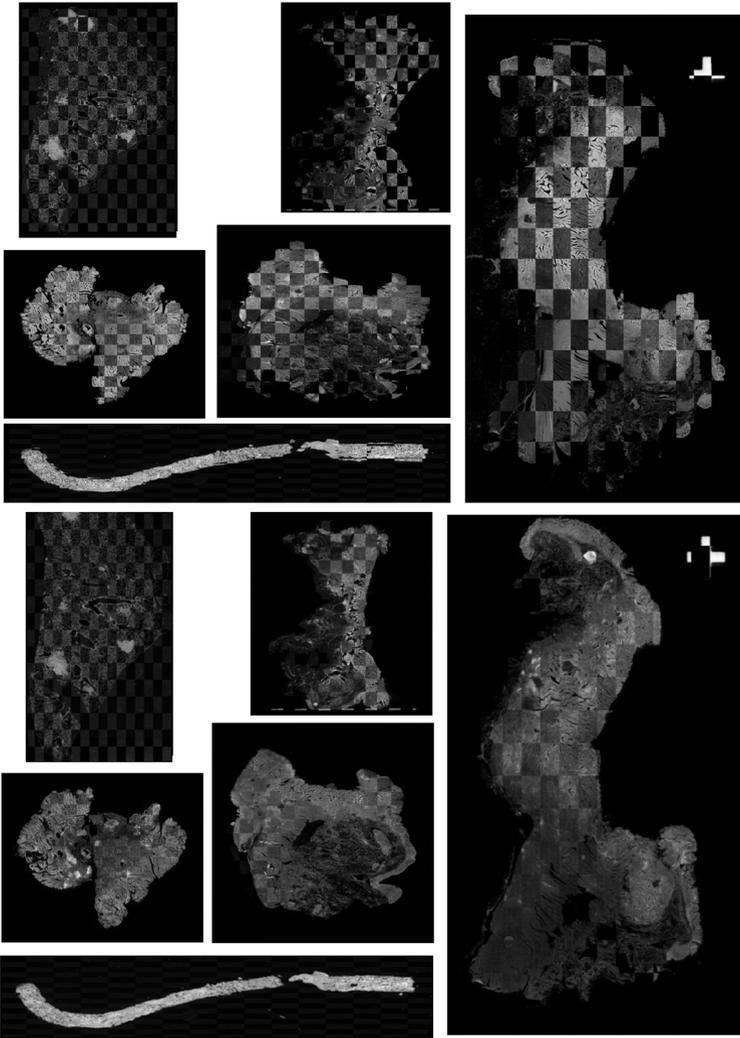
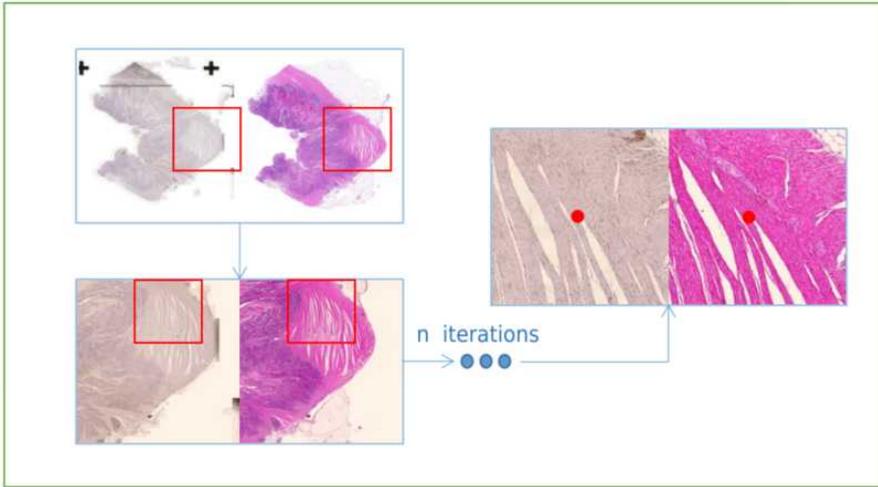
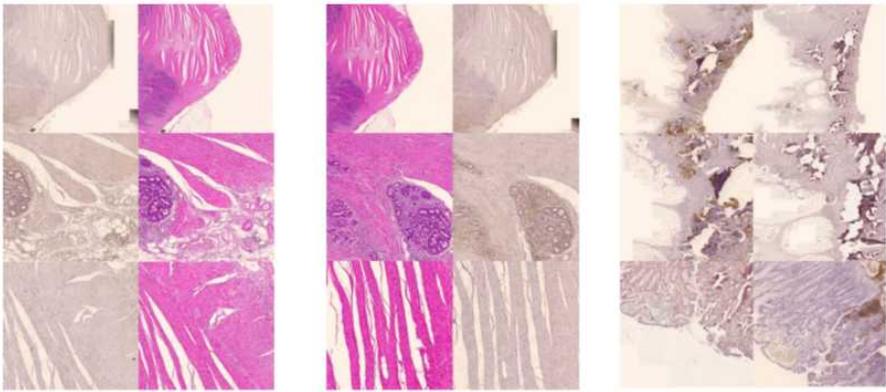


**Fig. 9** The figure shows the results of comparing the target image with the registered image, and the results are presented in the form of the checkerboard. The target image and the aligned image alternately appear in the figure. The registration results for the general contour and texture are excellent. The distinction between the source image and the target image is given in the first figure. The comparison between the transformed source image and the target image is illustrated in the second figure.

We compared the feature points obtained from a network based on deep learning features with traditional features. The evaluation was carried out on various datasets. It was observed that the deep learning-based approach had improved significantly compared to the traditional approach regarding the number of point pairs and reliability. Figure 2 depicts the impact of the comparison.



(a)



(b)

**Fig. 10** The image was down-sampled and cropped centered on the inferred points to get a new image for iterative inference. The above figure (a) depicts the iterative inference process. While the following figure (b) illustrates the pairs of patches constructed according to the iterative inference process.

Figure 2 displays the matching results of four distinct tissue pathology images using various point matching methods. The two rows above are the matching results of the traditional methods, SIFT and ORB, respectively. While the two rows below are the matching results of the two deep learning networks employed in this paper. It is apparent that the points derived from the two rows of images above are quite sparse and have a significant mismatch rate. Inversely, the matched point pairs generated using the deep learning approach cover the whole image and every part of the organization, allowing

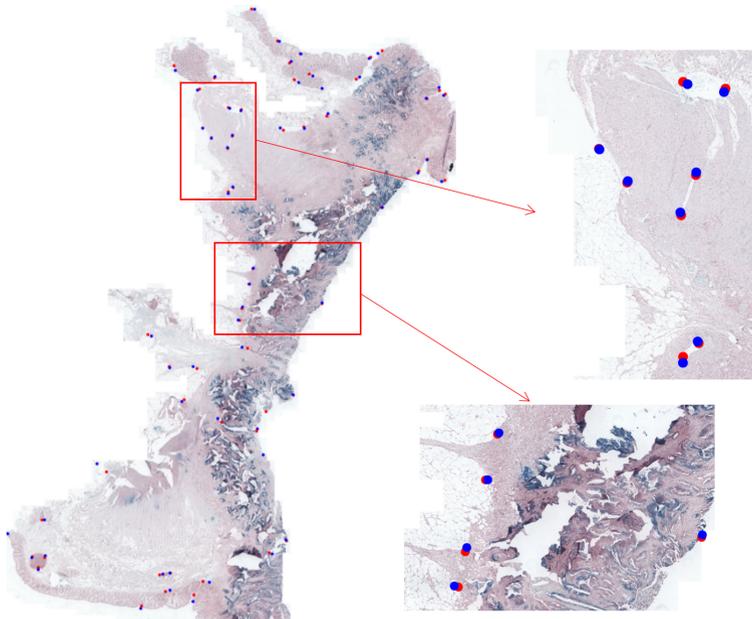


**Fig. 11** The alignment results are shown in the form of landmarks. The red dots are the results obtained by model inference, and the blue dots are ground-truth.

us to utilize these accurate and dense matched point pairs for interpolation to approximate the real DVF.

Figure 9 exhibits a checkerboard representation of our registration result. As demonstrated in the figure, the contours and internal textures of the registered image and the target image are extremely closely matched, and the junction of the checkerboard is quite smooth. We randomly selected a graph to compare the inference results with the landmark results in Figure 11. We found that our prediction of landmarks is highly accurate. We evaluate our results on the grand challenge website. Table 1 summarizes the test results as compared to other techniques. We only submitted the results from the pre-trained model without any targeted training. We found that our method has a significant advantage over other methods in terms of the median and the mean of rTRE. We also provide the outcomes just with matched network interpolation. According to the table, utilizing a single matching network has proven extremely competitive. Our total accuracy surpasses any other technique. The results in all data sets and the test set were provided. The method marked with \* in the table is a deep learning-based method that was trained in the training set. The rest are conventional methods.

After fine-tuning, our results have been further improved, as shown in table 2. The diagram below summarizes our results. And our results are

**Table 2** Quantitative results evaluated on the ANHIR dataset after fine-tuned

	Average-c	Average-Median rTRE	Median-Average rTRE	Median-Median rTRE	Max-Average rTRE	Max-Median rTRE
	ALL					
Ours*(train)	<b>0.0020</b>	<b>0.0012</b>	<b>0.0011</b>	0.0008	<b>0.0130</b>	<b>0.0047</b>
Ours	0.0035	0.0022	0.0025	0.0016	0.0258	0.0170
SuperPoint only	0.0056	0.0031	0.0032	0.0021	0.0397	0.0225
COTR only	0.0059	0.0028	0.0035	0.0019	0.0546	0.0245
SFG*(supervised)	0.0046	<b>0.0010</b>	0.0038	<b>0.0007</b>	0.0186	0.0073
SFG*	0.0081	0.0024	0.0069	0.0016	0.0284	0.0172
MEVIS	0.0043	0.0028	0.0028	0.0018	0.0251	0.0188
AGH	0.0073	0.0032	0.0036	0.0017	0.029	0.0214
UPENN	0.0041	0.0029	0.0029	0.0019	0.0238	0.0224
DeepHistReg*	0.0060	0.0033	0.0047	0.0019	0.0239	0.0224
CKVST	0.0042	0.0026	0.0027	0.0023	0.0239	0.0189
TUNI	0.0063	0.0031	0.0048	0.0021	0.0287	0.0204
	TEST					
Ours*(train)	<b>0.0034</b>	<b>0.0022</b>	<b>0.0023</b>	<b>0.0016</b>	<b>0.0240</b>	<b>0.0169</b>
Ours	0.0037	0.0023	0.0026	0.0017	0.0277	0.0183
SFG*(supervised)	0.0083	0.0025	0.0070	<b>0.0016</b>	0.0291	0.0181
SFG*	0.0082	0.0026	0.0070	0.0017	0.0286	0.0183
MEVIS	0.0044	0.0027	0.0029	0.0018	0.0251	0.0188
AGH	0.0072	0.0031	0.0057	0.0017	0.0251	0.0188
UPENN	0.0041	0.0029	0.0029	0.0019	<b>0.0239</b>	0.0190
DeepHistReg*	0.0061	0.0030	0.0047	0.0019	0.0276	0.0197
CKVST	0.0042	0.0026	0.0027	0.0023	0.0239	0.0189
TUNI	0.0063	0.0031	0.0048	0.0021	0.0287	0.02045

outstanding in practically every measure and achieved the state-of-the-art performance in the Average rTRE on the test dataset <sup>1</sup>. The rTRE (relative Target Registration Error) metric is calculated as follows:

$$rTRE = \frac{TRE}{\sqrt{w^2 + h^2}} \quad (10)$$

Where  $w$  and  $h$  are the image dimensions, TRE is the mean square error of the predicted and true values.

We compare the results with COTR alone and after using the outlier detection module to filter out the mismatching pairs in figure 12. Our modified model greatly improves the accuracy of the feature point matching model. It can be observed from the part in the red circle that the image without outlier detection has severe distortion, which heavily impacts the final accuracy and the availability of the registration network. After the outlier detection eliminates the false matches, the image distortion passing through the DVF vanishes and becomes flatter. It indicates that our statistical anomaly matching detection model is effective.

## 4 Discussion

The experimental results validate that our proposed hybrid feature-based deep learning registration framework overcomes the challenges of traditional feature matching. Our approach employs two deep learning feature networks that extract a denser set of feature points. In addition, the proposed outlier detection model effectively eliminates false matches. The effectiveness of the above methods is all quantitatively validated on the ANHIR dataset.

For the first time, we employed the approach of fine-tuning natural image pre-training models in medical image data to pathological image registration.

<sup>1</sup><https://anhir.grand-challenge.org/evaluation/challenge/leaderboard/>

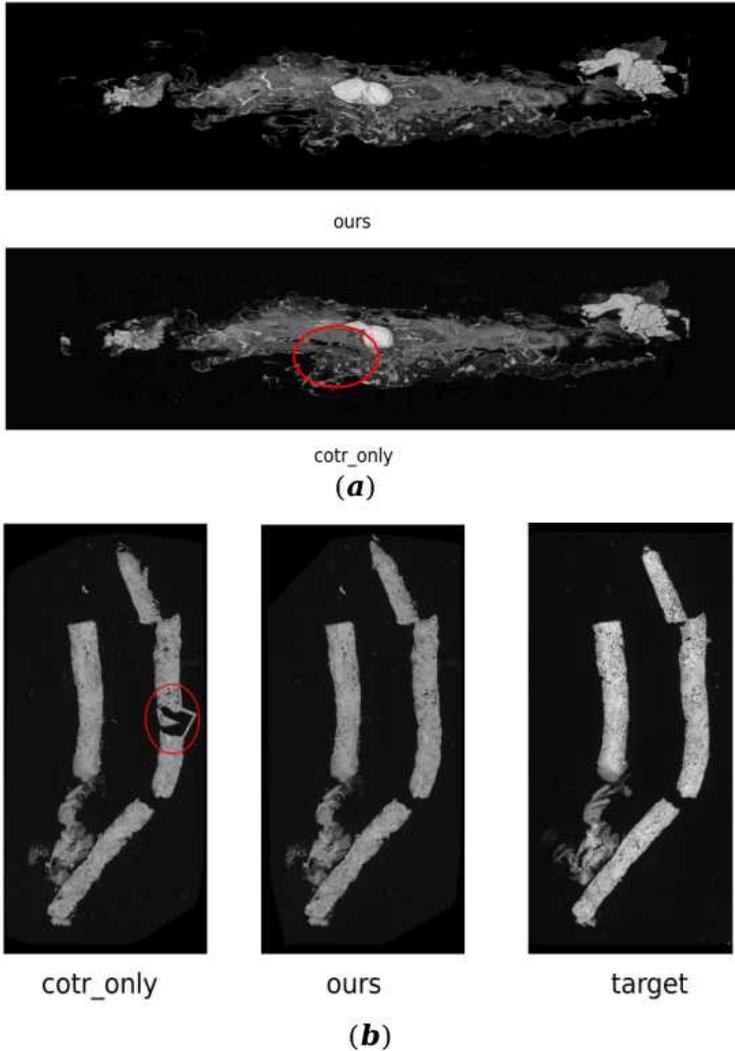


**Fig. 12** Figures (a) and (b) show the registration results using direct interpolation of COTR only. Compared with the results from the proposed framework, our method solves the image distortion problem caused by mismatch.

And it proved effective in the experiment, which shows that natural image pre-training model fine-tuning has great potential in medical images.

In our studies, we discovered that we could achieve fairly decent performance utilizing simply the pre-trained models from natural images without targeted training. It may be owing to the large dataset on natural images that makes powerful generalization feasible, which demonstrates whether it is permitted to remedy the deficiency of incomplete data in medical images by using a large number of natural pictures.

There are also several drawbacks to the proposed approach. First, we extract feature points and match them via a hybrid network, which results in a more complicated network structure. Consequently, our approach significantly fails to outperform conventional iteration-based algorithms in terms of computing efficiency. Second, regularization terms and differential analysis may restrict the DVF’s smoothness, preserving the image’s topology in deformation-based neural networks and conventional iteration-based methods. In contrast, if there is a mismatch, the feature point matching-based framework may ignore the image’s structure.

Our further work will be focused on improvement in two directions: (1) to design more lightweight networks; (2) to apply this framework to the situation of other medical images, such as CT, MRI, etc. We remark that the registration has a wide range of applications for the 3D medical image scenario, including assisted segmentation, tumor tracking, target area outlining, etc. Consequently, we intend to expand our deep feature registration network to 3D, contributing to improved accuracy in big deformation and multi-modal registration.

## 5 Conclusion

This paper proposes a novel registration network based on hybrid deep features. The proposed framework outperforms the current state-of-the-art methods in terms of accuracy. We particularly overcome the two feature point challenges of pair sparsity and mismatching as opposed to standard feature-based techniques. Moreover, our network achieves excellent results just by pre-training on natural images. After fine-tuning it, we get better results, which indicates that our approach is more generalizable and may be utilized for image registration in clinical and applications in medicine.

## Acknowledgments

This work is partly supported by grants from the National Natural Science Foundation of China (U20A201795, U21A20480, 61871374, 62001464), Young S&T Talent Training Program of Guangdong Provincial Association for S&T (SKXRC202224), and the Chinese Academy of Sciences Special Research Assistant Grant Program.

## Declarations

The authors declare that they have no known competing financial interests or personal relationships that could have appeared to influence the work reported in this paper.

## References

- [1] Wodzinski, M., Müller, H.: Deephistreg: Unsupervised deep learning registration framework for differently stained histology samples. *Computer Methods and Programs in Biomedicine* **198**, 105799 (2021)
- [2] Borovec, J., Kybic, J., Arganda-Carreras, I., Sorokin, D.V., Bueno, G., Khvostikov, A.V., Bakas, S., Eric, I., Chang, C., Heldmann, S., *et al.*: Anhir: automatic non-rigid histological image registration challenge. *IEEE transactions on medical imaging* **39**(10), 3042–3052 (2020)
- [3] Arganda-Carreras, I., Sorzano, C.O., Marabini, R., Carazo, J.M., Ortiz-de-Solorzano, C., Kybic, J.: Consistent and elastic registration of histological sections using vector-spline regularization. In: *International Workshop on Computer Vision Approaches to Medical Image Analysis*, pp. 85–95 (2006). Springer
- [4] Rueckert, D., Sonoda, L.I., Hayes, C., Hill, D.L., Leach, M.O., Hawkes, D.J.: Nonrigid registration using free-form deformations: application to breast mr images. *IEEE transactions on medical imaging* **18**(8), 712–721 (1999)
- [5] Avants, B.B., Epstein, C.L., Grossman, M., Gee, J.C.: Symmetric diffeomorphic image registration with cross-correlation: evaluating automated labeling of elderly and neurodegenerative brain. *Medical image analysis* **12**(1), 26–41 (2008)
- [6] Glocker, B., Sotiras, A., Komodakis, N., Paragios, N.: Deformable medical image registration: setting the state of the art with discrete methods. *Annual review of biomedical engineering* **13**, 219–244 (2011)
- [7] Klein, S., Staring, M., Murphy, K., Viergever, M.A., Pluim, J.P.: Elastix: a toolbox for intensity-based medical image registration. *IEEE transactions on medical imaging* **29**(1), 196–205 (2009)
- [8] Website, A.: ANHIR: automatic non-rigid histological image registration challenge. <https://anhir.grand-challenge.org>, 2019
- [9] Borovec, J., Munoz-Barrutia, A., Kybic, J.: Benchmarking of image registration methods for differently stained histological slides. In: *2018 25th IEEE International Conference on Image Processing (ICIP)*, pp. 3368–3372 (2018). IEEE
- [10] Lotz, J., Weiss, N., Heldmann, S.: Robust, fast and accurate: a 3-step method for automatic histological image registration. *arXiv preprint arXiv:1903.12063* (2019)

- [11] Zhao, S., Lau, T., Luo, J., Eric, I., Chang, C., Xu, Y.: Unsupervised 3d end-to-end medical image registration with volume tweening network. *IEEE journal of biomedical and health informatics* **24**(5), 1394–1404 (2019)
- [12] Wodzinski, M., Müller, H.: Unsupervised learning-based nonrigid registration of high resolution histology images. In: *International Workshop on Machine Learning in Medical Imaging*, pp. 484–493 (2020). Springer
- [13] Wodzinski, M., Müller, H.: Learning-based affine registration of histological images. In: *International Workshop on Biomedical Image Registration*, pp. 12–22 (2020). Springer
- [14] Liang, X., Li, N., Zhang, Z., Xiong, J., Zhou, S., Xie, Y.: Incorporating the hybrid deformable model for improving the performance of abdominal ct segmentation via multi-scale feature fusion network. *Medical Image Analysis* **73**, 102156 (2021)
- [15] Liang, X., Zhao, W., Hristov, D.H., Buyyounouski, M.K., Hancock, S.L., Bagshaw, H., Zhang, Q., Xie, Y., Xing, L.: A deep learning framework for prostate localization in cone beam ct-guided radiotherapy. *Medical Physics* **47**(9), 4233–4240 (2020)
- [16] Ma, J., Jiang, X., Fan, A., Jiang, J., Yan, J.: Image matching from hand-crafted to deep features: A survey. *International Journal of Computer Vision* **129**(1), 23–79 (2021)
- [17] Lowe, D.G.: Distinctive image features from scale-invariant keypoints. *International journal of computer vision* **60**(2), 91–110 (2004)
- [18] Rublee, E., Rabaud, V., Konolige, K., Bradski, G.: Orb: an efficient alternative to sift or surf 2011 international conference on computer vision. Barcelona, Spain: IEEE, 2564–2571 (2011)
- [19] Sun, J., Shen, Z., Wang, Y., Bao, H., Zhou, X.: Loftr: Detector-free local feature matching with transformers. In: *Proceedings of the IEEE/CVF Conference on Computer Vision and Pattern Recognition*, pp. 8922–8931 (2021)
- [20] DeTone, D., Malisiewicz, T., Rabinovich, A.: Superpoint: Self-supervised interest point detection and description. In: *Proceedings of the IEEE Conference on Computer Vision and Pattern Recognition Workshops*, pp. 224–236 (2018)
- [21] Tyszkiewicz, M., Fua, P., Trulls, E.: Disk: Learning local features with policy gradient. *Advances in Neural Information Processing Systems* **33**, 14254–14265 (2020)

- [22] Jiang, W., Trulls, E., Hosang, J., Tagliasacchi, A., Yi, K.M.: Cotr: Correspondence transformer for matching across images. In: Proceedings of the IEEE/CVF International Conference on Computer Vision, pp. 6207–6217 (2021)
- [23] Sarlin, P.-E., DeTone, D., Malisiewicz, T., Rabinovich, A.: Superglue: Learning feature matching with graph neural networks. In: Proceedings of the IEEE/CVF Conference on Computer Vision and Pattern Recognition, pp. 4938–4947 (2020)
- [24] Bay, H., Tuytelaars, T., Gool, L.V.: Surf: Speeded up robust features. In: European Conference on Computer Vision, pp. 404–417 (2006). Springer
- [25] Jiang, X., Ma, J., Xiao, G., Shao, Z., Guo, X.: A review of multimodal image matching: Methods and applications. *Information Fusion* **73**, 22–71 (2021)
- [26] Li, Z., Snavely, N.: Megadepth: Learning single-view depth prediction from internet photos. In: Proceedings of the IEEE Conference on Computer Vision and Pattern Recognition, pp. 2041–2050 (2018)
- [27] Lin, T.-Y., Maire, M., Belongie, S., Hays, J., Perona, P., Ramanan, D., Dollár, P., Zitnick, C.L.: Microsoft coco: Common objects in context. In: European Conference on Computer Vision, pp. 740–755 (2014). Springer
- [28] Dai, A., Chang, A.X., Savva, M., Halber, M., Funkhouser, T., Nießner, M.: Scannet: Richly-annotated 3d reconstructions of indoor scenes. In: Proceedings of the IEEE Conference on Computer Vision and Pattern Recognition, pp. 5828–5839 (2017)
- [29] Derpanis, K.G.: Overview of the ransac algorithm. *Image Rochester NY* **4**(1), 2–3 (2010)
- [30] Fischler, M.A., Bolles, R.C.: Random sample consensus: a paradigm for model fitting with applications to image analysis and automated cartography. *Communications of the ACM* **24**(6), 381–395 (1981)
- [31] Liu, F.T., Ting, K.M., Zhou, Z.-H.: Isolation forest. In: 2008 Eighth Ieee International Conference on Data Mining, pp. 413–422 (2008). IEEE
- [32] Liu, F.T., Ting, K.M., Zhou, Z.-H.: Isolation-based anomaly detection. *ACM Transactions on Knowledge Discovery from Data (TKDD)* **6**(1), 1–39 (2012)
- [33] Ge, L., Wei, X., Hao, Y., Luo, J., Xu, Y.: Unsupervised histological image registration using structural feature guided convolutional neural network. *IEEE Transactions on Medical Imaging* (2022)

- [34] Wodzinski, M., Skalski, A.: Automatic nonrigid histological image registration with adaptive multistep algorithm. arXiv preprint arXiv:1904.00982 (2019)
- [35] Venet, L., Pati, S., Yushkevich, P., Bakas, S.: Accurate and robust alignment of variable-stained histologic images using a general-purpose greedy diffeomorphic registration tool. arXiv preprint arXiv:1904.11929 (2019)